Sound & Vibration 2026, 60(5), 4310.
doi: https://doi.org/10.59400/sv4310

Article

Study of the mechanical behavior under compression of a tetrachiral auxetic tubular structure

Ali Bejaoui[1,2,*], Ltaief Lammari[3,*], Fethi Abbassi[4], Ali Trabelsi[2], Mohamed-Ali Rezgui[2]

[1] National School of Engineers of Tunis, University of Tunis El Manar, Tunis 1002, Tunisia

[2] Laboratory of Mechanics, Production and Energetics, Higher National Engineering School of Tunis, University of Tunis, Tunis 1008, Tunisia; ali.trabelsi@ensit.rnu.tn (AT); mohamedali.rezgui@esstt.rnu.tn (MAR)

[3] Mechanical and Agro-Industrial Engineering Laboratory, Higher School of Engineering of Medjez El Bab, University of Jendouba, Medjez El Bab 9070, Tunisia

[4] College of Engineering and Technology, American University of the Middle East, Egaila 54200, Kuwait; fethi.abbassi@aum.edu.kw

*** Corresponding author:** Ali Bejaoui, ali.bejaoui@isetb.rnu.tn; Ltaief Lammari, ltaief.laamari@esim.u-jendouba.tn

CITATION

Bejaoui A, Lammari L, Abbassi F, et al. Study of the mechanical behavior under compression of a tetrachiral auxetic tubular structure. Sound & Vibration. 2026; 60(5): 4310. https://doi.org/10.59400/sv4310

ARTICLE INFO

Received: 21 April 2026
Revised: 5 June 2026
Accepted: 14 July 2026
Available online: 14 August 2026

Abstract: Additive manufacturing enables the fabrication of architected materials with geometries unattainable through conventional processes. Among these, auxetic metastructures, characterized by a negative Poisson's ratio, have attracted considerable interest owing to their unusual deformation mechanisms and superior energy absorption and dissipation. This study investigates the mechanical behavior of a tetrachiral tubular structure made of AA7075-T651 aluminum alloy under axial compression, focusing on the influence of boundary conditions at the part–machine interfaces. Finite element simulations accounted for frictional contact, geometric nonlinearity, and the rotational kinematics of tetrachiral cells. The results reveal that friction governs the onset and magnitude of the auxetic response. Under highly constrained contact ($\mu = 0.8$), ligament rotation is suppressed, and the structure deforms conventionally, exhibiting a positive effective Poisson's ratio ($\nu \approx +0.28$), limited twisting (two turns), and a maximum compressive load of 3.877 kN. Reducing friction to $\mu = 0.2$ with a fixed base promotes in-plane node rotation, activating the tetrachiral mechanism and yielding $\nu \approx -0.25$, four turns, and a higher load of 3.883 kN. The most pronounced auxetic response arises when both ends are free to slide under low friction, producing $\nu \approx -0.32$, five turns, and an 8.2% contraction of the outer diameter. Across the investigated configurations, the effective Poisson's ratio varies by 0.60. These findings demonstrate that the auxetic behavior of tetrachiral tubes is highly sensitive to frictional and kinematic constraints, which must be carefully controlled to ensure reproducible mechanical performance.

Keywords: auxetic tubular structure; tetrachiral lattice; effective Poisson's ratio; finite element modeling; axial compression; boundary conditions; additive manufacturing

1. Introduction

In recent years, a new class of engineered materials, known as metamaterials, has emerged in the field of materials science [1,2]. The field of mechanical metamaterials has experienced significant growth over the past two decades, driven by the discovery that a structure's macroscopic mechanical behavior can be engineered to be largely independent of the intrinsic properties of its constituent material. While classical structural design is performed by choosing a material with desired stiffness, strength, and/or damping properties, the metamaterial concept focuses on the internal topology, such as the cell shape, cell connectivity, and the kinematics of the constituent ligaments, to achieve mechanical properties that are far beyond what the constituent material alone could ever offer. This shift in material design has been particularly successful in enabling mechanical properties that cannot be achieved using conventional materials. These include negative stiffness [3], negative compressibility [4], programmable anisotropy [5], and, most importantly for the present study, a negative Poisson's ratio. Since geometry can be decoupled from chemistry, structural design has thus become an optimization problem where the unit cell itself is the main parameter of design. What distinguishes metamaterials from other engineered materials is that their unique properties arise primarily from the design of their internal architecture rather than from their chemical composition. Auxetic materials are distinguished by their unconventional mechanical behavior, exhibiting a response that contrasts with the predictions of classical mechanics [3]. In contrast to the conventional behavior of isotropic solids, which become narrower under tensile loading and wider under compression, auxetic materials expand laterally when stretched and contract laterally when subjected to compressive loading [4,5]. Therefore, the geometric configuration of the microstructures in auxetic materials enables complex deformation mechanisms and intricate kinematic interactions [6]. When auxetic cellular structures are subjected to external loading, the cells' geometry initiates spatial deformation, allowing for a negative Poisson's ratio of the structure and expansion or contraction of the material in two orthogonal axes. The literature describes several classes of auxetic architectures, each exhibiting a distinct deformation mechanism that underpins the negative Poisson's ratio phenomenon [7]. Honeycombs are auxetic by virtue of the hinge-like flexure of the cell ribs. Re-entrant honeycombs demonstrate auxeticity by having angled cell walls that straighten out under tension and collapse more under compression. Rotating-square or rotating-triangle tessellations are composed of rigid units joined by pin joints that rotate in opposite directions to form an expanding/contracting network. Chiral and anti-chiral lattices, of which the tetrachiral topology analysed in the current paper is a member, obtain auxeticity via the synergistic rotation of central nodes which wind and unwind the connecting ligaments around the node periphery. In contrast to re-entrant or rotating-unit designs, chiral lattices exhibit in-plane rotation coupled with an intense twisting motion if realized in the form of a tubular structure, which associates axial compression with a torsional response and an actual three-dimensional shrinkage of the cross-section. This extra twisting degree of freedom makes chiral tubes very promising for the design of structures with prescribed values of the axial stiffness, the torsional compliance, and the radial contraction; on the other hand, it significantly increases the degree to which their effective mechanical response is influenced by the manner in which the structure is loaded and constrained at its boundaries.

Given that auxetic architectures provide significant advantages in multiple areas, interest in this type of structure has increased rapidly. In aerospace applications, for example, their ability to absorb energy makes them highly desirable. In biomedical applications, auxetic materials can provide even distribution of loads across implants or prosthetic devices [8, 9]. Additionally, they hold promise for use as vibration isolators, shock absorbers in mechanical systems, and even as multifunctional devices such as piezoelectric systems [10, 11]. The increasing use of additive manufacturing processes has contributed to the widespread use of auxetic materials, as it enables the manufacture of complex 3D geometric structures [12–14]. In particular, powder-bed and laser-based additive processes provide the possibility to produce auxetic lattices and tubular metastructures directly in high-performance metallic alloys, thus effectively removing the tradeoff that previously forced designers to choose between elaborate chiral geometries and load-bearing structural alloys. The present work focuses on the 7xxx series aluminum alloy AA7075-T651, which combines a high strength-to-weight ratio with excellent fatigue resistance. These attributes make it an attractive candidate for energy-absorbing aerospace and automotive components, where auxetic tubes could replace conventional crash boxes or honeycomb cores. Tetrachiral tubular structures in particular are largely employed in industry because of their low weight, high specific modulus, high energy dissipation features, and good damping behavior [15]. The deformation mechanism of these tubular structures is primarily dictated by the tangential arrangement of the ligaments linking the central ring-shaped nodes. When subjected to axial compression, the rigid nodes undergo synchronised rotation, causing the interconnecting ligaments to progressively wrap or unwrap around the nodes. This kinematic interaction generates coupled twisting and axial contraction of the tube, resulting in a well-defined and highly predictable deformation mode under idealised conditions [16]. Although the geometry of a structure is generally the primary factor governing its deformation behavior, a considerable degree of uncertainty can arise from the boundary conditions imposed during experimental testing [17]. The clamping method, the friction conditions at the contact interfaces, and the alignment of the specimen are among the key factors that influence the extent to which the measured data accurately represent the specimen's actual deformation behavior [18]. This discrepancy stems from the constraint conditions introduced by contact interfaces, which differ from the idealised assumptions of theoretical models. For instance, friction at the specimen–platen interface generates shear forces that oppose the tube's natural radial expansion at its ends [19]. As a result, friction constrains specimen rotation and displacement, ultimately influencing its overall deformation behavior. A high friction coefficient, for example, will limit the rotation of the ligaments and prevent the structure from functioning in its typical chiral fashion. On the other hand, an excessively high level of constraint may lead to localized plastic deformations in the specimen [20]. In the broader literature on cellular and lattice structures, this pronounced sensitivity to contact conditions is commonly referred to as the ”boundary-layer effect”, describing the localised region near the specimen ends where the periodic deformation of the bulk lattice is disrupted because the unit cells cannot deform as freely as those within the interior. For chiral tubes, the boundary layer is expected to be particularly pronounced because their deformation relies on coordinated node rotation propagating along the tube height. Any constraint that locally inhibits this rotation extends the boundary layer inward, reducing the volume of material exhibiting the auxetic mechanism and, consequently, lowering the effective Poisson's ratio measured from the global diameter and height changes. Therefore, the effective Poisson's ratio and mechanical response are influenced by both the specimen architecture and the experimental setup.

The study aimed to examine the effects of friction and boundary conditions on the compressive behavior of tetrachiral auxetic tubes [21–23]. Furthermore, structural deformation, quantified by the number of node rotations, and the effective Poisson's ratio were evaluated to determine the effects of the geometric parameters. This enhances the understanding of the relationship between microstructure, testing conditions, and material performance, which is essential for the design of efficient auxetic metamaterials [24].

The remainder of the paper is structured as follows. Section 2 describes the materials, specimen design, experimental setup, and finite element methodology adopted to investigate the compressive behavior of tetrachiral auxetic tubes under different friction and boundary conditions. Section 3 presents and discusses the experimental and numerical results, with particular emphasis on the effects of friction and boundary constraints on deformation mechanisms, structural rotations, the effective Poisson's ratio, and the overall mechanical response. Finally, the conclusion (Section 4) summarises the main findings and outlines potential directions for future research.

2. Materials and methods

2.1. Theoretical framework

Poisson's ratio is a fundamental parameter describing material deformation. Under uniaxial loading, it is defined as the negative ratio of transverse strain to axial strain. In auxetic structures, this quantity is commonly reported as an effective Poisson's ratio, reflecting the geometry-dependent deformation of the structure. In the case of axial compression applied along the z-direction, the effective Poisson's ratio of the structure can be stated as in Equation (1) [25]:

$$\begin{gathered} \nu_{eff}(t) = -\frac{\varepsilon_r(t)}{\varepsilon_z(t)} \\ \varepsilon_r(t) = \frac{d(t)-d_0}{d_0}, \varepsilon_z(t) = \frac{h(t)-h_0}{h_0} \end{gathered} \tag{1}$$

where $\varepsilon_r(t)$ is the instantaneous radial strain (variation of the external diameter) and $\varepsilon_z(t)$ is the instantaneous axial strain (variation of the height), and d_0 and h_0 are the initial diameter and height, and $d(t)$ and $h(t)$ their values at time t. These quantities are obtained from direct geometric measurements during the loading process [26].

Poisson's ratio in auxetic materials can be negative, and this implies that radial and axial strains are of the same sign. The physical interpretation is that, under a negative ε_z value (corresponding to axial compression of the tube), the radial strain εr is also negative. Consequently, the outer diameter of the tube decreases simultaneously with its length, rather than expanding laterally as would occur in conventional materials exhibiting a positive Poisson's ratio. Therefore, the effective Poisson's ratio defined above should not be considered a classical material property, as it is neither constant nor intrinsic to the material. Instead, it represents an instantaneous, configuration-dependent parameter that varies with the applied axial strain and evolves according to the changing number of winding layers during the loading process.

In linear elastic theory, the infinitesimal strain tensor can be expressed as in

Equation (2) [26,27]:

$$\varepsilon_{ij} = \frac{1}{2}\left(\frac{\partial u_i}{\partial x_j} + \frac{\partial u_j}{\partial x_i}\right) \tag{2}$$

where u_i is the displacement field.

For an isotropic elastic material, the linear stress–strain relationship is expressed as in Equation (3) [28,29].

$$\begin{gathered} \sigma_{ij} = 2\mu\,\varepsilon_{ij} + \lambda\,\varepsilon_{kk}\,\delta_{ij} \\ \mu = \tfrac{E}{2(1+\nu_0)},\ \lambda = \tfrac{E\,\nu_0}{(1+\nu_0)(1-2\nu_0)} \end{gathered} \tag{3}$$

where μ denotes the shear modulus, λ the Lamé parameter, and δ_{ij} the Kronecker delta.

The present work examines a tetrachiral tubular structure made of AA7075-T651 aluminum alloy. Considering the significant role of plastic deformation in its mechanical response, the material behavior is modeled using the Johnson–Cook constitutive formulation, which accounts for the effects of strain hardening, strain-rate sensitivity, and thermal softening. The yield stress is given in Equation (4) [30].

$$\sigma_y = \left(A + B\,\varepsilon_p^n\right)\left(1 + C\ln\dot{\varepsilon}^*\right)\left(1 - T^{*m}\right) \tag{4}$$

where ε_p is the equivalent plastic strain, $\dot{\varepsilon}^*$ the normalised strain rate, and T^* the homologous temperature. The parameters A, B, n, C, and m correspond to experimental calibration.

For quasi-static compressive loading at room temperature, the temperature term becomes $T^* = 0$, and the expression simplifies to Equation (5) [29].

$$\sigma_y = \left(A + B\,\varepsilon_p^n\right)\left(1 + C\ln\dot{\varepsilon}^*\right) \tag{5}$$

Upon formulating the dynamic equilibrium equations and discretizing the system within the finite element framework, the resulting governing equation is obtained as presented in Equation (6) [31].

$$[M]\{\ddot{u}\} + [C]\{\dot{u}\} + [K]\{u\} = \{F\} \tag{6}$$

where $[M]$, $[C]$, and $[K]$ correspond to the system mass, damping, and stiffness matrices, respectively, and $\{u\}$, $\{\dot{u}\}$, and $\{\ddot{u}\}$ are the nodal displacement, velocity, and acceleration vectors, respectively, resulting from the finite element discretization.

Since the structure undergoes geometric and material nonlinear deformations, the equilibrium equations are solved through an incremental and iterative approach, allowing the nonlinear response to be captured over the complete loading history.

2.2. Numerical methodology

The geometry of the tetrachiral honeycomb tube is constructed from a representative elementary unit cell, as illustrated in **Figure 1a,b**. This unit cell is periodically repeated along the circumferential direction to form a closed chiral ring structure. Subsequently, n_{cc} identical rings are stacked axially, perpendicular to the cross-sectional plane, resulting in the formation of the complete tetrachiral tubular metastructure, as depicted in **Figure 1c**.

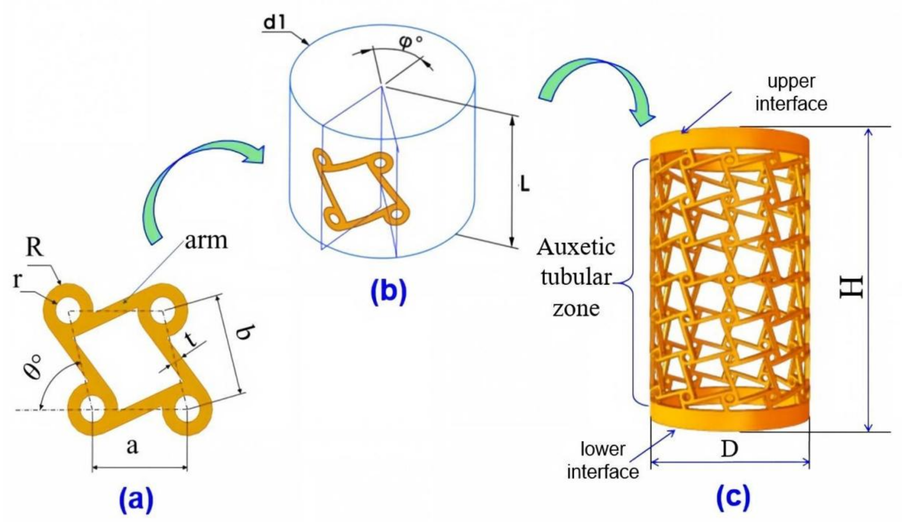

Figure 1. Tetrachiral honeycomb auxetic tubular structure: **(a)** Section parameters; **(b)** Angular parameters; **(c)** 3D model.

To guarantee geometric continuity and structural stability during the loading process, two additional chiral rings were incorporated at both ends of the tube. Different configurations of the tetrachiral architecture were subsequently generated by varying the characteristic geometric parameters and the orientation of the unit cell. This parametric approach enables a systematic investigation of the influence of architectural features on the overall mechanical response and facilitates the optimization of the structural performance.

The metastructure is modeled as being made of AA7075-T651 aluminum alloy, whose mechanical and physical properties are: Young's modulus $E = 70$ GPa, Poisson's ratio $\nu = 0.3$, and density $\rho = 2,700$ kg/m^3 [32]. The tube exhibits a constant wall thickness (e) of 2 mm. Its vertical extent results from the linear stacking of eight unit cells ($n_{cc} = 8$), yielding a total height of 150 mm. Circumferentially, fourteen cells are distributed around an outer diameter of 75 mm.

The reliability of the numerical simulations depends heavily on the appropriate formulation of the finite element model and the accurate definition of the loading conditions. Several critical aspects, including mesh density, boundary conditions, kinematic constraints, and loading characteristics, must be carefully considered to ensure a realistic representation of the structural response. In this study, a series of quasi-static axial compression simulations was performed to investigate the energy absorption capability, auxetic behavior, global mechanical response, and deformation mechanisms of the tetrachiral metastructure. Particular emphasis was placed on evaluating the effects of frictional interactions and boundary constraints at the contact interfaces between the tube and the loading plates. The structural domain was discretized using 12,679 quadratic tetrahedron solid elements (C3D10) to accurately model the stress and strain fields throughout the structure. This discretization ensures an effective representation of the local and global mechanical response, enabling accurate prediction of stress concentrations, deformation patterns, and the overall structural behavior under compressive loading. To reproduce the axial compression test, two rigid loading plates, each governed by a reference node, were positioned at the ends of the tetrachiral tube. The lower plate was fixed in all degrees of freedom, while the upper plate was free to move only in the axial direction under a prescribed displacement, thereby reproducing quasi-static axial compression, as illustrated in **Figure 2**.

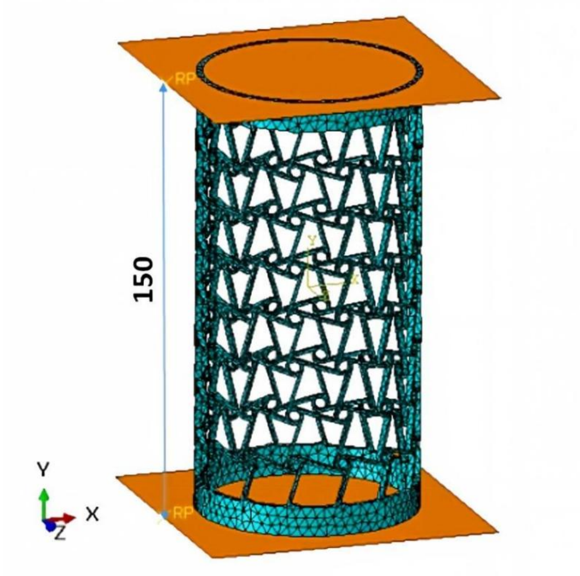

Figure 2. Geometric configuration used in the numerical simulations.

To examine the sensitivity of the finite element simulations, a mesh convergence analysis was performed before the parametric investigation. The meshing procedure was progressively refined until negligible variations were observed in both the load–displacement response and the computed effective Poisson's ratio, thereby demonstrating mesh-independent numerical results. Both the coarse and the medium meshes led to a much stiffer elastic response and slightly underestimated the maximum load, while the results from the medium and fine meshes were within 5% in terms of the peak load and the effective Poisson's ratio. Therefore, the intermediate mesh is kept for subsequent computations, since it balances the accuracy requirements and the computational time. A global contact algorithm with finite-sliding capability was employed to model the contact interactions between the tetrachiral tube and the rigid loading plates. In addition, self-contact between adjacent ligaments was activated to prevent nonphysical interpenetration during large compressive deformations associated with chiral rotation. The constitutive behavior of the material was described using the Johnson–Cook model, with parameters previously calibrated through experimental testing. To quantify the individual and combined effects of interface friction and boundary constraints on the mechanical response of the tetrachiral tube, three finite element configurations of the same structure were investigated. The configurations differed only in the friction coefficient and the constraint conditions imposed at the limiting contact interface, while all other modeling parameters remained unchanged.

- Configuration 1 (0.8 LF UF): $\mu = 0.8$, lower interface free (LF), and upper interface free (UF).
- Configuration 2 (0.2 LC UF): $\mu = 0.2$, lower interface constrained (LC), and upper

interface free (UF).

- Configuration 3 (0.2 LF UF): $\mu = 0.2$, lower interface free (LF), and upper interface free (UF).

These configurations enable the individual and combined effects of interface friction and geometric constraints to be isolated, thereby providing a comprehensive assessment of their influence on the energy absorption capacity, auxetic response, and deformation kinematics of the tetrachiral tubular metastructure under quasi-static axial compression.

3. Results and discussion

Figure 3 compares the load–displacement responses obtained under the three boundary condition configurations. Despite the differences in contact and constraint conditions, all configurations exhibit a characteristic two-stage mechanical response, reflecting the progressive evolution of the deformation mechanisms in the tetrachiral metallic tube during quasi-static axial compression.

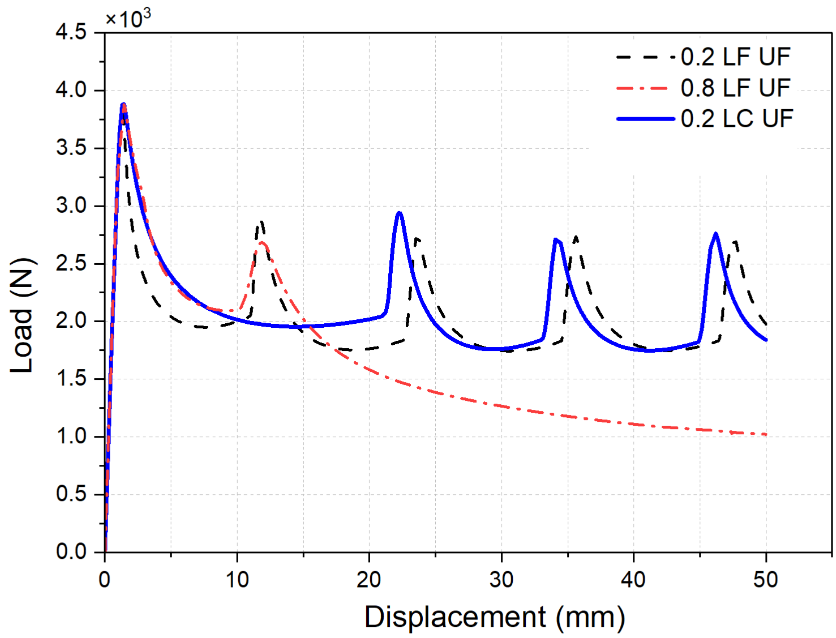

Figure 3. Load–displacement curves for the three configurations.

In the initial elastic regime, all configurations exhibit an almost identical linear load–displacement response up to the first peak load, indicating that the structural stiffness is essentially unaffected by the interface conditions. The complete overlap of the curves in this region demonstrates that neither the friction coefficient nor the imposed boundary constraints has a significant influence on the initial elastic response of the tetrachiral tube. Within this small-deformation domain, the rings and ligaments deform predominantly because of elastic bending/stretching without significant rotation around the main axis, explaining the insensitivity of the structural stiffness to boundary constraints. Beyond the initial peak load, all configurations exhibit a significant reduction in the load-carrying capacity, indicating the onset of plastic deformation. This stage is characterized by the progressive plastic bending and rotation of the ligaments about the vertical axis, which initiate the characteristic deformation mechanism governing the compressive response of the tetrachiral architecture. As compression continues, the combined effects of geometric nonlinearity and material hardening induce cyclic sequences of load increases and decreases, each corresponding to the formation of a new winding in the adjacent ring. **Table 1** summarizes the effective Poisson's ratio, number of turns, diameter variation, and maximum load for all configurations. The successive peaks and valleys observed in the load–displacement curves constitute the characteristic signature of the energy absorption process in the tetrachiral tube.

Table 1. Effective Poisson's ratio, number of turns, diameter variation, and maximum load for all configurations.

Configuration	μ	v_{eff}	Windings	Diameter reduction	Maximum load (kN)
0.8 LF UF	0.8	≈+0.28	2	Negligible	3.877
0.2 LC UF	0.2	≈−0.25	4	~6%	3.883
0.2 LF UF	0.2	≈−0.32	5	~8.2%	3.877

This oscillatory response is governed by the kinematic rotational freedom permitted by the imposed boundary conditions. Each load drop corresponds to a discrete winding event, during which the elastic strain energy accumulated within a ring of ligaments is suddenly released once a critical rotation threshold is reached. Beyond this limit, the ligaments undergo rapid reconfiguration into a wound state, after which the applied load is progressively transferred to the adjacent ring, where the energy accumulation and release cycle is repeated along the tube height. Hence, the magnitude and the frequency of these oscillations represent, in a single curve, the energy lost on each event and the number of rings that can perform a complete winding motion. Frictional constraints that limit the rotation of the nodes will produce fewer and shallower load drops since only a small number of rings can attain the rotation maximum that is necessary to activate a winding event before the structure succumbs to a more conventional, bending-dominated mode of deformation. On the other hand, low friction and free-end configurations enable the winding front to advance along almost the entire tube length, leading to a longer series of pronounced load oscillations that is the cause of the larger winding counts observed in those cases.

3.1. Effect of boundary conditions on the mechanical response

Boundary conditions play a fundamental role in governing the mechanical response of cellular and auxetic structures by influencing load transfer, deformation kinematics, and contact interactions. In the present study, the effects of interface friction and geometric constraints are investigated through three finite element configurations subjected to quasi-static axial compression. Their influence on the load–displacement response, energy absorption capability, auxetic behavior, and deformation mechanisms is systematically evaluated to elucidate the contribution of each boundary condition to the overall structural performance of the tetrachiral tubular metastructure.

- **Configuration 1 (0.8 LF UF)**

Under high interface friction, the tetrachiral tube exhibits significant radial contraction from the onset of axial compression, as shown in **Figure 4**. As deformation progresses, localized buckling develops within the ligaments, progressively restricting their ability to rotate about the vertical axis. The high-friction constraint inhibits the characteristic chiral rotation mechanism, limiting the deformation process to two winding events and promoting a deformation mode dominated by axial shortening. Consequently, the effective Poisson's ratio remains positive ($\nu_{eff} \approx 0.28$), indicating a conventional, non-auxetic response. Under these conditions, the structure attains a maximum load of 3.877 kN.

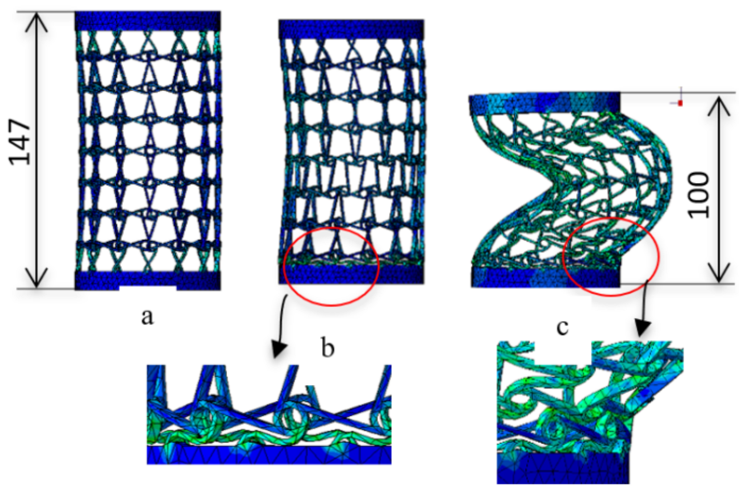

Figure 4. Configuration (1): Coefficient of friction 0.8 with both the upper and lower tube ends unconstrained.

- **Configuration 2 (0.2 LC UF)**

In this configuration, the combination of a constrained bottom ring and a low friction coefficient produces a pronounced asymmetry in the deformation pattern (**Figure 5**). The overall deformation pattern is similar to that observed in configuration 3, but with substantially enhanced three-dimensional rotational motion. Owing to the fully constrained base, rotational deformation is concentrated in the upper rings, where three of the four structural windings are observed, as shown in **Figure 5**. Consequently, the effective Poisson's ratio becomes negative ($\nu_{eff} \approx -0.25$), indicating the onset of auxetic behavior, with a diameter variation of approximately 6%, confirming the activation of the auxetic mechanism. The maximum compressive load reaches 3.883 kN.

- **Configuration 3 (0.2 LF UF)**

In this configuration, reduced friction combined with fully free ends provides maximal kinematic freedom (**Figure 6**). During the initial stage of compression, the tube undergoes radial contraction. As the compressive strain increases, however, severe deformation of the upper ligaments promotes a localized increase in diameter, although the overall structure continues to exhibit a net radial contraction of approximately 8.2%. Five structural windings are recorded, the highest among all investigated configurations, demonstrating the ability of the ligaments to undergo successive rotations along the tube height. Consequently, this configuration exhibits the most negative effective Poisson's ratio with a value of $\nu_{eff} \approx -0.32$, indicating the onset of auxetic behavior. However, the peak compressive load of 3.877 kN remains almost constant compared with the previous configuration.

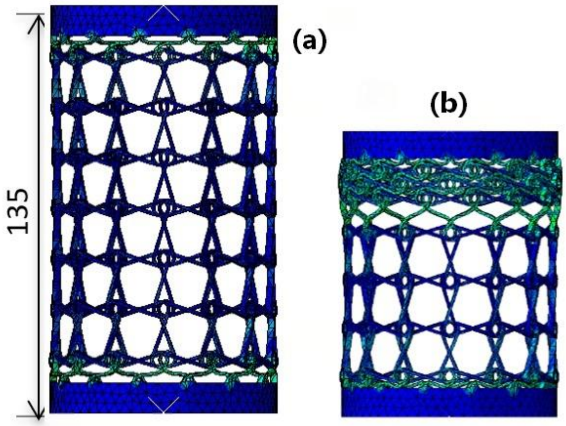

Figure 5. Configuration (3): Coefficient of friction 0.2, with the bottom ring blocked and the top ring unconstrained: **(a)** Initial stage with radial shrinkage; **(b)** Large deformation with localized diametral increase.

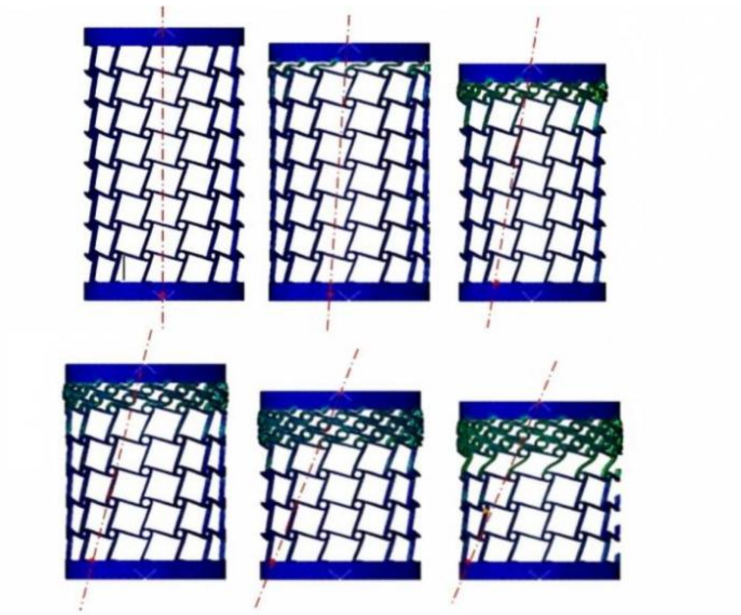

Figure 6. Configuration (2): Friction coefficient 0.2, and both lower and upper rings are unconstrained; five turns with complete deformation and maximum auxeticity.

3.2. Boundary-controlled auxetic behavior

The comparative assessment demonstrates that the auxetic response of the tetrachiral tube is primarily governed by the interface conditions, even though the intrinsic material properties remain important. At high friction levels, the structure undergoes quasi-axial deformation with radial contraction, resulting in a positive Poisson's ratio, similarly to conventional materials. The study showed that under low friction and free boundaries, a coordinated chiral winding mechanism is switched on and results in radial expansion with a negative Poisson's ratio (from −0.25 to −0.32) along with axial deformation. The geometric constraint at the bottom interface inhibits node rotation locally in the lower rings, but the free top interface allows nodes of the upper rings to rotate and wind, resulting in a deformation mode that combines conventional and auxetic characteristics. This observation confirms the conclusion that the friction coefficient and the end-fixation condition are two separate design parameters and, as such, can be optimized independently based on the unit-cell geometry to achieve a particular combination of stiffness, auxetic response and energy-absorption capability relevant to a specific application. The effective Poisson's ratio varies substantially across the configurations (1–3), ranging from +0.28 to −0.32, demonstrating that auxetic behavior is not an intrinsic property of the structure geometry but rather a latent kinematic response, which is governed by the boundary conditions and the available rotational freedom. This interpretation is further supported by the consistency of the number of structural windings, peak compressive load, and diameter evolution. These findings show a high correlation between boundary constraints, deformation mechanisms, and the onset of auxetic behavior. This is in line with experimental and numerical analyses of related chiral and re-entrant structures that have also found that the effective Poisson's ratio measured on a finite sample can be significantly different from the value calculated for an infinite periodic lattice where the frictional and loading conditions were taken into account [33]. The study has extended this understanding to the specific case of a tetrachiral tube subjected to axial compression, demonstrating that a single geometry and material system can exhibit a broad spectrum of mechanical responses solely through modifications to the interface conditions. These findings highlight the critical role of boundary conditions in governing the deformation mechanism and enabling the transition from conventional to auxetic behavior. The pronounced sensitivity of the tetrachiral tube to interface conditions has important implications for both experimental characterization and structural design. In laboratory testing, friction, platen surface roughness, and boundary constraints should be carefully controlled and explicitly reported, as they can shift the effective Poisson's ratio of the same specimen from strongly auxetic to conventional behavior. Conversely, this sensitivity provides an effective design parameter. Since friction and boundary constraints can be tailored independently of the unit-cell geometry through surface treatments, engineered contact interfaces, or rotational fixtures, the mechanical response can be adjusted after fabrication without modifying the underlying geometry. This enables the development of tunable auxetic structures with controllable Poisson's ratio and energy-absorption capability. Such adaptability is particularly attractive for protective systems, crashworthy components, and deployable aerospace structures, where different stages of operation may require either compliant auxetic behavior or higher structural stiffness.

4. Conclusions

This study carried out a numerical investigation aiming to understand how boundary conditions at the part–machine interface impact the effective Poisson's ratio and overall mechanical response of a tetrachiral tubular metastructure subjected to quasi-static axial compression. The results demonstrate that the auxetic behavior of the structure is not an intrinsic material property but relates to the degree of kinematic freedom allowed by the interface. Under high friction (μ = 0.8), rotational mobility is almost fully suppressed, resulting in predominantly axial deformation along with a radial contraction and early buckling. Only two windings form, and the structure behaves similarly to a conventional material with a slightly positive effective Poisson's ratio ($\nu_{eff} \approx +0.28$) and a maximum load of 3.877 kN. In contrast, low-friction configurations (μ = 0.2) promote significant rotational freedom and enable the development of the characteristic chiral winding mechanism. The fixed-base/free-apex configuration produces four windings and intermediate auxeticity ($\nu_{eff} \approx -0.25$) with a 6% diameter reduction and a peak load of 3.883 kN. When both ends are free, the structure reaches its highest level of kinematic mobility, forming five windings and achieving the most negative Poisson's ratio ($\nu_{eff} \approx -0.32$) and the largest diameter reduction (8.2%), with a maximum load of 3.877 kN. The progression in both winding count (from 2 to 5) and Poisson's ratio (+0.28 to −0.32) reflects the intensification of the auxetic mechanism induced by reduced friction and geometric freedom.

This study has provided valuable insights for the design of tetrachiral metastructures, revealing that auxeticity is an interface mechanics-driven phenomenon, which can be strengthened, weakened, or encoded. These results pave the way for creating smart materials and systems with tunable mechanical response that do not require change of the material composition or intrinsic geometry, with potential applications in adaptive, morphing, and energy dissipative systems. Beyond the quasi-static conditions considered in this study, several research directions warrant further investigation, including the effects of strain rate, impact loading, multiaxial loading, geometric variations, and material nonlinearities on the auxetic response of tetrachiral tubes. Further extensions may include: (1) The integration of the developed finite element framework with experimental compression tests on additively manufactured specimens of AA7075-T651. This would enable direct validation of the predicted friction-dependent transition from conventional to auxetic behavior while quantifying the range of friction coefficients attainable for practical metallic contact interfaces. (2) Extending the parametric study to dynamic and impact loading could determine whether the boundary-condition sensitivity observed under quasi-static compression persists at high strain rates, thereby providing valuable insights for the design of crashworthy and protective structures based on tetrachiral tubes. (3) Investigating the effects of unit-cell parameters (ligament length, node radius, wall thickness, and the number of circumferential and axial cells), together with friction and end constraints, could enable the development of surrogate models to predict the effective Poisson's ratio and load-carrying capacity of tetrachiral tubes without requiring full nonlinear finite element simulations. Such models would facilitate the optimization and design of lightweight auxetic structures for targeted stiffness-to-weight ratios, controlled radial contraction, and enhanced energy absorption.

Author contributions: Conceptualization, AB, MAR and FA; methodology, AB and LL; software, AB; validation, AB, LL and MAR; formal analysis, AB; investigation, AB; data curation, AB and LL; writing—original draft preparation, AB and LL; writing—review and editing, FA, MAR and AT; visualization, AB; supervision, MAR and FA. All authors have read and agreed to the published version of the manuscript.

Funding: This work received no external funding.

Institutional review board statement: Not applicable.

Informed consent statement: Not applicable.

Data availability statement: The data used in this study are available from the corresponding author upon reasonable request.

Conflict of interest: The authors declare no conflict of interest.

AI use statement: The authors declare that no artificial intelligence (AI) tools were used in the preparation of this manuscript.

References

1. Kumar R, Kumar M, Chohan JS, et al. Overview on metamaterial: History, types and applications. Materials Today: Proceedings. 2022; 56: 3016–3024. doi: 10.1016/j.matpr.2021.11.423
2. Ni X, Yves S, Krasnok A, et al. Topological metamaterials. Chemical Reviews. 2023; 123(12): 7585–7654. doi: 10.1021/acs.chemrev.2c00800
3. Zheng X, Zhang X, Chen TT, et al. Deep learning in mechanical metamaterials: From prediction and generation to inverse design. Advanced Materials. 2023; 35(45): 2302530. doi: 10.1002/adma.202302530
4. Bao Y, Wei Z, Jia Z, et al. Mechanical metamaterial design with the customized low-frequency bandgap and negative Poisson's ratio via topology optimization. Extreme Mechanics Letters. 2024; 67: 102124. doi: 10.1016/j.eml.2024.102124
5. Bohara RP, Linforth S, Nguyen T, et al. Anti-blast and impact performances of auxetic structures: A review of structures, materials, methods, and fabrications. Engineering Structures. 2023; 276: 115377. doi: 10.1016/j.engstruct.2022.115377
6. Mora S, Pugno NM, Misseroni D. 3D printed architected lattice structures by material jetting. Materials Today. 2022; 59: 107–132. doi: 10.1016/j.mattod.2022.05.008
7. Rahimi-Lenji A, Heidari-Rarani M, Mirkhalaf M, et al. On the internal architecture of lightweight negative Poisson's ratio (auxetic) metastructures: A review. Materials & Design. 2025; 260: 115225. doi: 10.1016/j.matdes.2025.115225
8. Benedetti M, du Plessis A, Ritchie RO, et al. Architected cellular materials: A review on their mechanical properties towards fatigue-tolerant design and fabrication. Materials Science and Engineering: R: Reports. 2021; 144: 100606. doi: 10.1016/j.mser.2021.100606
9. Zadpoor AA. Mechanical performance of additively manufactured meta-biomaterials. Acta Biomaterialia. 2019; 85: 41–59. doi: 10.1016/j.actbio.2018.12.038
10. Hu Y, Fan Y, Wu Y, et al. A piezoelectric damping support for the vibration suppression of rotors. In: Fu S (editor). 2023 Asia-Pacific International Symposium on Aerospace Technology (APISAT 2023), Proceedings of the APISAT: Asia-Pacific International Symposium on Aerospace Technology; 16–18 October 2023; Lingshui, China. Springer; 2024. pp. 1237–1256. doi: 10.1007/978-981-97-3998-1_97
11. Nazir A, Abate KM, Kumar A, et al. A state-of-the-art review on types, design, optimization, and additive manufacturing of cellular structures. The International Journal of Advanced Manufacturing Technology. 2019; 104(9): 3489–3510. doi: 10.1007/s00170-019-04085-3
12. Dananjaya SAV, Chevali VS, Dear JP, et al. 3D printing of biodegradable polymers and their composites—Current state-of-the-art, properties, applications, and machine learning for potential future applications. Progress in Materials Science. 2024; 146: 101336. doi: 10.1016/j.pmatsci.2024.101336
13. Khan N, Riccio A. A systematic review of design for additive manufacturing of aerospace lattice structures: Current trends and future directions. Progress in Aerospace Sciences. 2024; 149: 101021. doi: 10.1016/j.paerosci.2024.101021
14. Xin X, Liu L, Liu Y, et al. 4D printing auxetic metamaterials with tunable, programmable, and reconfigurable mechanical properties. Advanced Functional Materials. 2020; 30(43): 2004226. doi: 10.1002/adfm.202004226
15. Ding A, Tang F, Alsberg E. 4D printing: A comprehensive review of technologies, materials, stimuli, design, and emerging applications. Chemical Reviews. 2025; 125(7): 3663–3771. doi: 10.1021/acs.chemrev.4c00070

16. Zhang X, Yin J, Ren X, et al. Pre-torsion tubular metamaterials: Multi-effect integration of compression-torsion and auxetic behaviors for advanced functional applications. Advanced Science. 2025; 12(42): e12564. doi: 10.1002/advs.202512564
17. An R, Ge X, Wang M. Design and microscale fabrication of negative Poisson's ratio lattice structures based on multi-scale topology optimization. Machines. 2023; 11(5): 519. doi: 10.3390/machines11050519
18. Wang P, Fu X, Li C, et al. Research on a broadband vibration energy acquisition method combining nonlinear softening and hardening. Sound & Vibration. 2025; 59(2): 1712. doi: 10.59400/sv1712
19. Simpson J, Kazancı Z. Crushing investigation of crash boxes filled with honeycomb and re-entrant (auxetic) lattices. Thin-Walled Structures. 2020; 150: 106676. doi: 10.1016/j.tws.2020.106676
20. Etemadi S, Hosseinabadi M, Gholikord M, et al. Dynamic performance of arc-shaped auxetic structures through split Hopkinson pressure bar tests. Smart Materials and Structures. 2025; 34(8): 085022. doi: 10.1088/1361-665X/adf928
21. Jiang W, Ren X, Wang SL, et al. Manufacturing, characteristics and applications of auxetic foams: A state-of-the-art review. Composites Part B: Engineering. 2022; 235: 109733. doi: 10.1016/j.compositesb.2022.109733
22. Luo HC, Ren X, Zhang Y, et al. Mechanical properties of foam-filled hexagonal and re-entrant honeycombs under uniaxial compression. Composite Structures. 2022; 280: 114922. doi: 10.1016/j.compstruct.2021.114922
23. Li X, Peng W, Wu W, et al. Auxetic mechanical metamaterials: From soft to stiff. International Journal of Extreme Manufacturing. 2023; 5(4): 042003. doi: 10.1088/2631-7990/ace668
24. Zhang Y, Jiang WZ, Jiang W, et al. Recent advances of auxetic metamaterials in smart materials and structural systems. Advanced Functional Materials. 2025; 35(23): 2421746. doi: 10.1002/adfm.202421746
25. Ting TCT, Chen T. Poisson's ratio for anisotropic elastic materials can have no bounds. The Quarterly Journal of Mechanics and Applied Mathematics. 2005; 58(1): 73–82. doi: 10.1093/qjmamj/hbh021
26. Grédiac M, Sur F, Blaysat B. The grid method for in-plane displacement and strain measurement: A review and analysis. Strain. 2016; 52(3): 205–243. doi: 10.1111/str.12182
27. Gurtin ME, Fried E, Anand L. The Mechanics and Thermodynamics of Continua. Cambridge University Press; 2010. doi: 10.1017/CBO9780511762956
28. Gao XL. A new Timoshenko beam model incorporating microstructure and surface energy effects. Acta Mechanica. 2015; 226(2): 457–474. doi: 10.1007/s00707-014-1189-y
29. Selvadurai APS. On Spencer's displacement function approach for problems in second-order elasticity theory. Mathematics and Mechanics of Solids. 2023; 28(1): 56–92. doi: 10.1177/10812865221096771
30. Lenihan D, Ronan W, O'Donoghue PE, et al. A review of the integrity of metallic vehicle armour to projectile attack. Proceedings of the Institution of Mechanical Engineers, Part L: Journal of Materials: Design and Applications. 2019; 233(1): 73–94. doi: 10.1177/1464420718759704
31. Habte B. Matrix Structural Analysis and the Finite Element Methods Using Scilab and Octave: A Problem-Solving Approach. CRC Press; 2024. doi: 10.1201/9781003329350
32. Mohamed AB, Znaidi A, Daghfas O, et al. Evolution of mechanical behavior of aluminium alloy Al 7075 during maturation time. International Journal of Technology. 2016; 7(6): 1077–1085. Available online: https://ijtech.eng.ui.ac.id/article/view/358
33. Chow ZP, Gliszczyński A. Influence of boundary conditions on the residual compressive strength of impacted thin-walled GFRP channel section profiles. Composite Structures. 2025; 370: 119399. doi: 10.1016/j.compstruct.2025.119399